

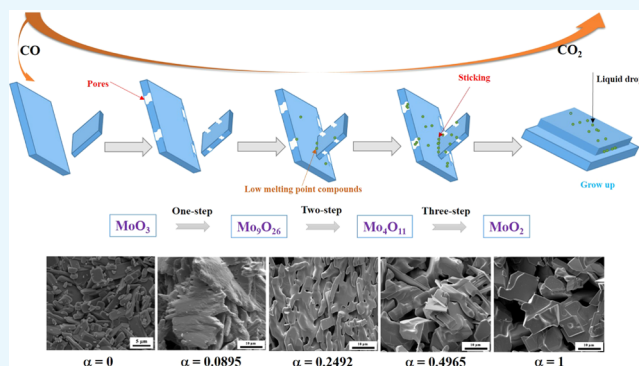
Mechanism and Kinetic Study of Reducing MoO₃ to MoO₂ with CO–15 vol % CO₂ Mixed Gases

Lu Wang,^{*,†,‡,§} Zheng-Liang Xue,^{*,†,‡} Ao Huang,[†] and Fang-Fang Wang[§]

[†]The State Key Laboratory of Refractories and Metallurgy and [‡]Key Laboratory for Ferrous Metallurgy and Resources Utilization of Ministry of Education, Wuhan University of Science and Technology, Wuhan 430081, Hubei, China

[§]School of Materials Science and Engineering, Beihang University, Beijing 100191, China

ABSTRACT: In the present paper, the reduction reaction of high-purity MoO₃ with CO–15 vol % CO₂ mixed gases in the temperature range of 901–948 K is investigated via the thermogravimetric analysis technology. The results show that reduction of MoO₃ to MoO₂ follows a three-step reaction process, viz., MoO₃ is first reduced into Mo₉O₂₆, followed by Mo₄O₁₁, and finally to MoO₂. The reaction sequences of MoO₃ → Mo₉O₂₆ → Mo₄O₁₁ → MoO₂ are proposed, which are quite different from those observed on reduction of MoO₃ by pure H₂ or CO gases. Pure Mo₉O₂₆ and Mo₄O₁₁ could be synthesized once suitable time was controlled. Rate-controlling steps for the reduction from MoO₃ to Mo₉O₂₆ and Mo₉O₂₆ to MoO₂ (include both Mo₉O₂₆ to Mo₄O₁₁ and Mo₄O₁₁ to MoO₂) are interfacial chemical reactions, with the activation energies of 318.326 and 112.047 kJ/mol, respectively. This study also discovers that the as-synthesized MoO₂ keeps the same platelet-shaped and smooth morphology as the MoO₃ raw material; however, its particles size gradually increased as the reaction proceeds due to the formation of low-melting-point eutectic and the sticking of different particles.



1. INTRODUCTION

Molybdenum dioxide (MoO₂) possesses a high melting point (>2773 K)¹ and density (6.47 g/cm³)² and a low oxygen content, which have made it become a potential Mo source for the direct alloying steelmaking or production of ferromolybdenum alloys.³ Compared to molybdenum trioxide (MoO₃; melting point: 1068 K; density: 4.692 g/cm³),^{4,5} MoO₂ will not sublime at the normal steelmaking temperature (1773 K) and could increase the transport or smelting process, which will further increase the yield of molybdenum (Mo) greatly. Therefore, the preparation of MoO₂ has attracted much attention in recent years and many routes have been developed. These routes include hydrogen reduction (reduction of MoO₃ with pure H₂),^{6,7} water vapor oxidation (oxidation of molybdenum sulfide concentrate with water vapor),^{8,9} and solid-phase reaction (roasting of mixed MoS₂ and MoO₃ powders).^{10,11} As for the gas–solid reaction, H₂ gas as the reducing agent has been widely studied,^{6,7} and pure CO gas was also adopted in our previous work.¹² However, CO–15 vol % CO₂ mixed gases as the reducing gases have never been used before. In this paper, one of the purposes is to explore a new approach for the preparation of MoO₂, so pure H₂ or CO was not adopted, and then the CO–15 vol % CO₂ mixed gases were used instead.

Recently, synthesis of tungsten carbides (W₂C) by the reduction–carburization of MoO₃ with different reducing gases has been widely reported.^{13–16} However, related study

for the preparation of molybdenum carbides (Mo₂C), especially for the use of CO as the reducing gas, was lacking.¹⁷ In our previous work,¹⁸ CO gas was first adopted to produce Mo₂C by using MoO₃ as the raw material, in which it was discovered that the preparation processes mainly proceeded following two stages: the reduction of MoO₃ to MoO₂ and the carburization from MoO₂ to Mo₂C. The characterizations of the intermediate product MoO₂ having great influences on those of the final product Mo₂C were also concluded. To avoid the occurrence of carbon deposition reaction, as shown in eq 1, a certain volume fraction of CO₂ was also added into the reducing gases. It was found¹² that when the volume fraction of CO₂ is about 15 vol %, the reaction kinetics curve is very similar to that of pure CO in the initial period; in the latter period, the reaction rate is still very rapid, which is much faster than that obtained by using pure CO due to the inhibiting effect of carbon deposition reaction, and then pure MoO₂ or Mo₂C could be easily obtained. When the volume fraction of CO₂ increased to 30 vol % or more, however, the reaction rate will be decreased largely, which was not beneficial for the preparation of MoO₂. Therefore, CO–15 vol % CO₂ mixed gases were selected for the preparation of MoO₂ in the current paper, which could also be used for the preparation of Mo₂C. Furthermore, the reduction mechanism and kinetics of

Received: September 26, 2019

Accepted: November 5, 2019

Published: November 15, 2019

MoO₃ to MoO₂ by H₂ have been widely studied.^{19–22} However, related studies for the reaction processes of MoO₃ to MoO₂ or MoO₃ to Mo₂C by CO–15 vol % CO₂ mixed gases were extremely scarce. To understand the whole reaction processes from MoO₃ to Mo₂C, the reduction mechanism and kinetics of MoO₃ to MoO₂ were studied first, which could also act as a preliminary work for the preparation of Mo₂C



As mentioned above, one of the current objectives is to develop a new and simple method for the preparation of MoO₂ with the use of CO–CO₂ mixed gases (CO–15 vol % CO₂ mixed gases are selected as the reducing gases due to the good inhibiting effect on the carbon deposition reaction and the rapid reaction rate). At the same time, the reduction mechanism and kinetics of MoO₃ to MoO₂ by the CO–15 vol % CO₂ mixed gases are illustrated, which will further give a better understanding on the reduction–carburization mechanism from MoO₃ to Mo₂C.

2. RESULTS

2.1. Thermogravimetric-Differential Thermal Analysis (TG-DTA) Experiments. The mass loss ratio (defined as W_t) of high-purity MoO₃ reduced by CO–15 vol % CO₂ mixed gases was calculated by eq 2

$$W_t = -\frac{m_t - m_0}{m_0} \times 100\% \quad (2)$$

where m_0 and m_t are the masses of initial sample and that reduced for a period of time t , respectively.

Reduction extent (defined as α) of the sample was calculated as the ratio of mass loss ratio W_t to the theoretical maximum mass loss ratio W_{\max} as shown in eq 3

$$\alpha = \frac{W_t}{W_{\max}} \times 100\% \quad (3)$$

2.1.1. Nonisothermal TG-DTA Experiments. Figure 1 shows the nonisothermal TG curves of reducing high-purity MoO₃ with CO–15 vol % CO₂ mixed gases from room temperature to 1550 K under four different heating rates: 5, 10, 15, and 20 K/min. From Figure 1, it can be clearly seen that the total reaction processes can be divided into three different stages with respect to the heating rates of 5, 10, and 15 K/min. The first stage is in

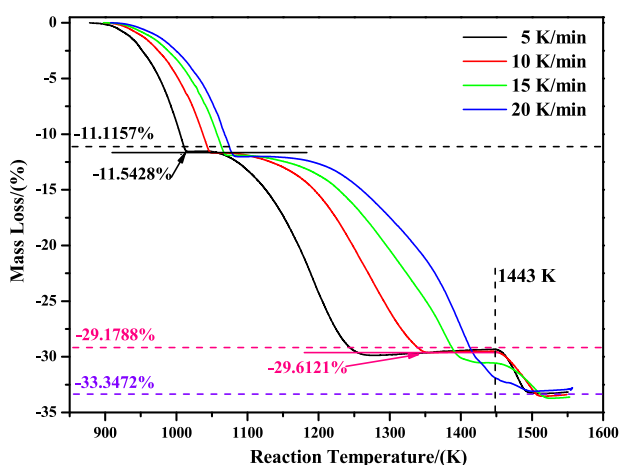
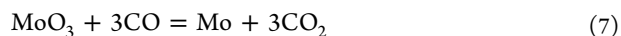
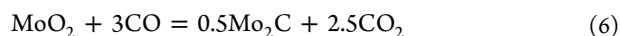
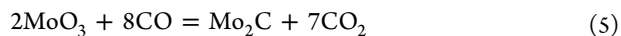
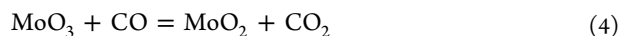


Figure 1. TG curves of reducing high-purity MoO₃ with CO–15 vol % CO₂ mixed gases under different heating rates (5, 10, 15, and 20 K/min).

the range of mass loss ratio from zero to –11.5428%, which is almost consistent with –11.1157% (corresponding to the mass change from MoO₃ to MoO₂, as shown in eq 4). Therefore, it can be deduced that the main reaction is the reduction of MoO₃ to MoO₂ in the first stage. The mass loss ratio for the second stage is –29.6121%, which is almost in good agreement with –29.1788% (corresponding to the mass change from MoO₃ to Mo₂C, as shown in eq 5). If considering the newly as-formed MoO₂ as the reactant, then the main reaction in the second stage is the reduction of MoO₂ to Mo₂C, as shown in eq 6. The third stage is the final platform section, corresponding to the mass loss ratio of –33.3472%, which is exactly equal to the theoretical maximum mass loss ratio from MoO₃ to metallic Mo, as shown in eq 7. As for the case of 20 K/min, however, the TG curve is a little different from the above three cases (this experiment at the heating rate of 20 K/min was conducted twice, and the results are almost the same). The first stage is almost the same as the lower heating rates (5, 10, and 15 K/min), that is, the mass loss ratio is also from zero to –11.5428%; as the temperature increases, the second and third stages are nearly overlapped and no obvious stable region existed; however, the final mass loss ratio is still equal to –33.3472%. All in all, it can be concluded that reduction of MoO₃ with CO–15 vol % CO₂ mixed gases can be divided into three main stages in the temperature range of room temperature to 1550 K: the first is from MoO₃ to MoO₂, then from MoO₂ to Mo₂C, and finally to generate metallic Mo



The nonisothermal thermogravimetric-differential thermal analysis (TG-DTA) curves at the heating rate of 10 K/min are also plotted and shown in Figure 2, which may contribute to the

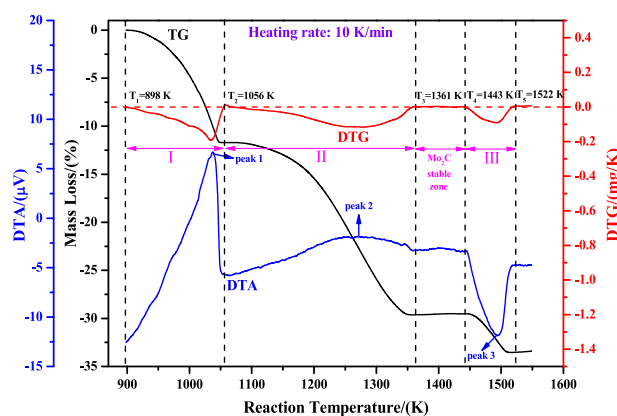


Figure 2. Nonisothermal TG-DTA curves of reducing high-purity MoO₃ with CO–15 vol % CO₂ mixed gases at the heating rate of 10 K/min.

deeper understanding of the reaction processes. From the DTA curve (denoted by the blue line), it can be known that reduction from MoO₃ to MoO₂ is an intense exothermic reaction, as seen by the sharp exothermic peak 1. Besides, the exothermic reaction from MoO₂ to Mo₂C can also be obtained, as seen by the broad exothermic peak 2. As to the third stage (from Mo₂C to metallic Mo), a sharp endothermic peak 3 is obviously observed, which

suggests that the process from Mo₂C to Mo is an endothermic reaction. Furthermore, from the DTG curve (denoted by the red line), the beginning (defined as T_1) and ending reaction temperatures (defined as T_2) from MoO₃ to MoO₂ can be obtained, i.e., $T_1 = 898$ K, $T_2 = 1056$ K (at the points for the values of DTG equal to zero). Accordingly, the ending reaction temperature from MoO₂ to Mo₂C (defined as T_3) and the beginning and ending reaction temperatures from Mo₂C to Mo (defined as T_4 and T_5 , respectively) can also be known, i.e., $T_3 = 1361$ K, $T_4 = 1443$ K, and $T_5 = 1522$ K. Similarly, the corresponding values for the heating rates of 5, 15, and 20 K/min can also be obtained, as listed in Table 1.

Table 1. Beginning and Ending Reaction Temperatures for Each Stage during the Total Reduction Processes in the Temperature Range of Room Temperature to 1550 K at Different Heating Rates

heating rate (K/min)	temperature (K)				
	T_1	T_2	T_3	T_4	T_5
5	888	1019	1283	1443	1507
10	898	1056	1361	1443	1522
15	904	1079	1425	1445	1528
20	907	1085			1502

From Table 1, it can be known that T_1 , T_2 , and T_3 all increased with increasing heating rate. The larger the heating rate is, the higher the beginning and ending reaction temperatures will be. T_1 is in the range of 888–907 K, which is larger than that of reducing industrial-grade MoO₃ with pure CO as the reducing gas (827 K).¹² The reasons for the increased temperature are due to the different raw materials and different reducing gases (CO–15 vol % CO₂ mixed gases vs pure CO). However, it can be clearly seen that the T_4 values are almost equal to each other for the heating rates of 5, 10, and 15 K/min, at a temperature of about 1443 K. From Figures 1 and 2, it can be found that a stable zone for Mo₂C (the result of X-ray diffraction (XRD) pattern is not given) always existed in those cases, which may provide enough time for the heat transport. Once the reaction temperature achieves, Mo₂C will begin to proceed the next reaction. As to T_5 , it is also increased with the increasing heating rate from 5 to 15 K/min. Due to the fact that T_3 is increased with the increasing heating rate, however, T_4 was almost constant (about 1443 K in the current paper). So, when the heating rate was further increased to 20 K/min, T_3 will be further increased and even almost equaled T_4 , and then the two stages (from MoO₂ to Mo₂C, and then to metallic Mo) will be overlapped to approximate one stage, which would lead to T_5 a little lower than those obtained at lower heating rates and the different kinetic curves, as shown in Figure 1.

2.1.2. Isothermal TG Experiments. One of the purposes of the current study was to provide a new route for the preparation of high-purity MoO₂. So, temperatures in the range of T_1 to T_2 shown in Table 1 were selected for the isothermal experiments. In this paper, temperatures of 901, 916, 932, and 948 K were adopted, and the corresponding experimental results are displayed in Figure 3 (the mass loss ratio curves have converted to the relationship between reaction extent and reaction time for convenience of the following kinetics analysis). It can be easily seen from this figure that the reaction extent depends strongly on the reaction temperature. The higher the reaction temperature is, the faster the reaction rate will be. Also, an obvious inflection point can be seen in the kinetic curves at the reaction

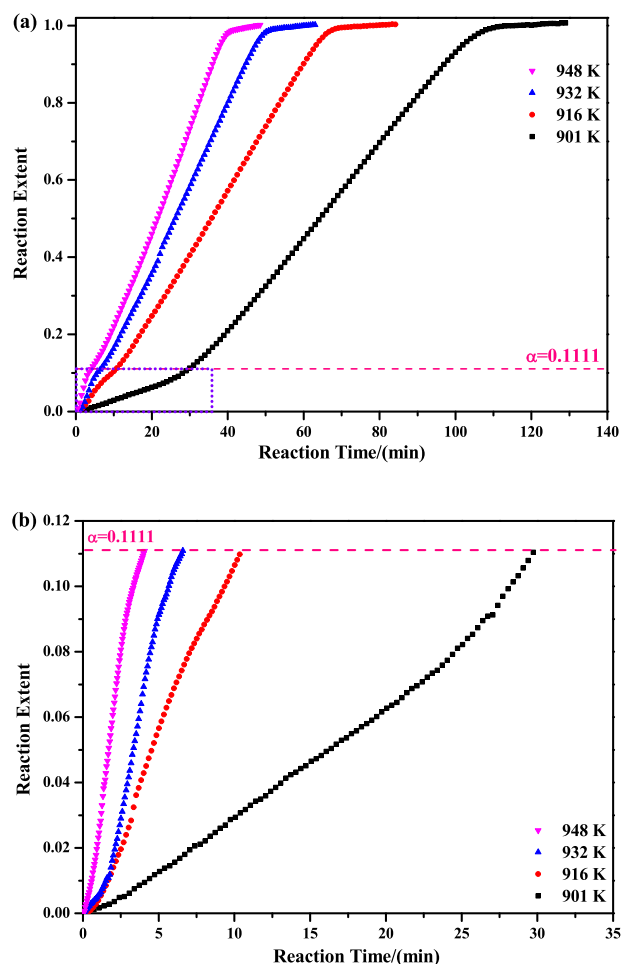
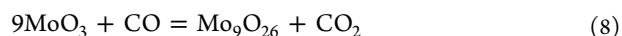


Figure 3. Isothermal TG curves of reducing high-purity MoO₃ with CO–15 vol % CO₂ mixed gases at 901, 916, 932, and 948 K (b) is the amplified image of the purple rectangles marked in (a).

extent of about 0.1111, which is in good agreement with the mass change from MoO₃ to Mo₉O₂₆, as expressed by eq 8. The generation of Mo₉O₂₆ can be further proved in the following XRD sections. Meanwhile, the reaction extent has an obvious linear relationship with reaction temperature, which can also be seen both in the stages from 0 to 0.1111 and 0.1111 to 1. The slopes in the stage from 0 to 0.1111 are more sensitive than those in the stage from 0.1111 to 1 (temperature is more beneficial for the increase of reaction rate in the stage from 0 to 0.1111 than that from 0.1111 to 1).



2.2. XRD Analyses. Figure 4 shows the XRD patterns of reaction products obtained by reducing high-purity MoO₃ completely with CO–15 vol % CO₂ mixed gases at the four different temperatures. The results showed that MoO₂ (PDF card No. 32-671) is always the only final product without other impurities, which is in good agreement with the kinetic curves shown in Figure 3a.

To clarify the phase-transition laws during the reaction processes, XRD patterns of samples obtained at different reaction extents were also detected. In this paper, 932 K is selected as the studied temperature, and $\alpha = 0.0286$, 0.0895, 0.2492, 0.4965, 0.8473, and 1 were chosen as the analyzed reaction extents, as indicated in Figure 5.

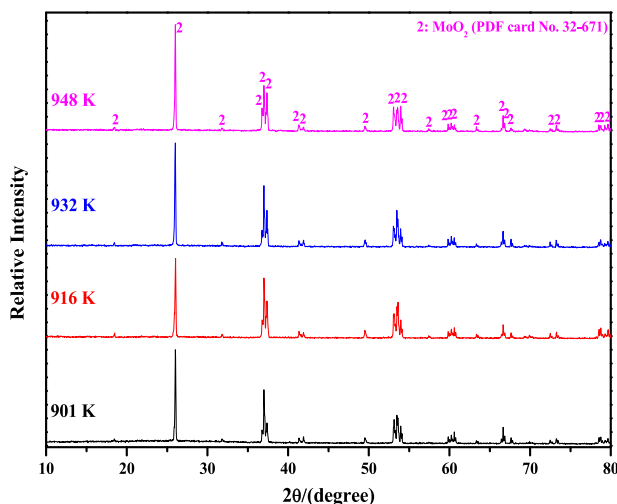


Figure 4. XRD patterns of reaction products obtained by reducing high-purity MoO_3 completely with CO –15 vol % CO_2 mixed gases at 901, 916, 932, and 948 K.

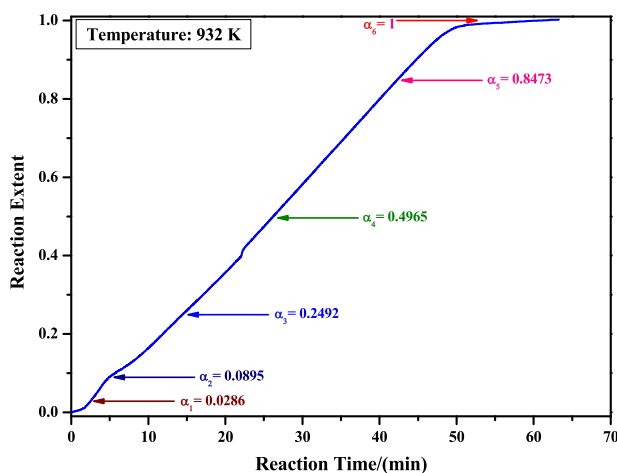


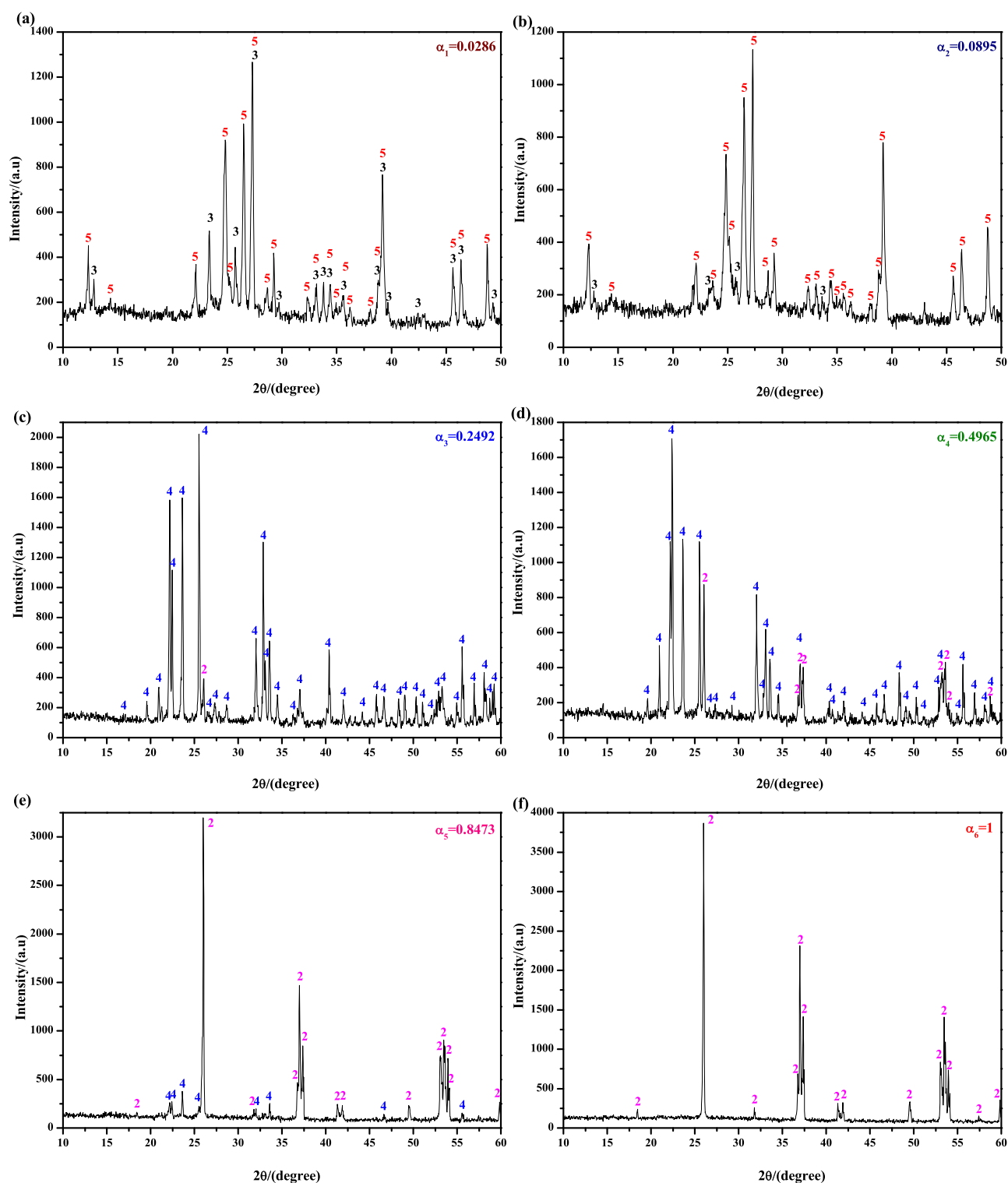
Figure 5. Isothermal TG curve of reducing high-purity MoO_3 with CO –15 vol % CO_2 mixed gases at 932 K. The directions indicated by the arrows are the as-prepared samples for the following XRD and field emission scanning electron microscopy (FE-SEM) analyses.

Figure 6 shows the XRD results of reaction products obtained according to Figure 5. When the reaction extent is $\alpha_1 = 0.0286$, most of the MoO_3 raw materials are reduced to Mo_9O_{26} (PDF card No. 12-753), which is a new intermediate product and not found in pure H_2 or CO reduction of MoO_3 to MoO_2 .^{7,12} As the reduction continues ($\alpha_2 = 0.0895$), MoO_3 nearly disappeared, and then the main product turns to be Mo_9O_{26} , as shown in Figure 6b, which can be seen clearer in Figure 7. Combining Figure 6a,b, it can be deduced that the main reaction is reducing MoO_3 to Mo_9O_{26} in the preliminary stage (α in the range of 0–0.0895), which agrees well with the results (α in the range of 0–0.1111) shown in Figure 3. When the reaction extent achieves 0.2492, however, both MoO_3 and Mo_9O_{26} suddenly disappeared and then the products are replaced by Mo_4O_{11} (PDF card No. 5-337); the formation of Mo_4O_{11} was also found in refs 7, 12 where pure H_2 or CO were used as the reducing gases. Besides, a small peak for MoO_2 is also detected, which indicates that MoO_2 is also formed in this situation, as shown in Figures 6c and 7. After that, the main peaks of Mo_4O_{11} and MoO_2 are monotonously decreased and increased, respectively, as shown in Figure 6d,e.

When the reduction reaction is complete ($\alpha_6 = 1$), the products are all composed of MoO_2 , as shown in Figure 6f. Therefore, it can be inferred that reduction from Mo_9O_{26} to Mo_4O_{11} is very rapid and could hardly be controlled. Thus, the main reaction in the latter period (α in the range of 0.1111–1) is the reduction of Mo_4O_{11} to MoO_2 .

2.3. FE-SEM Examinations. The typical micrographs of reaction products obtained by reducing high-purity MoO_3 completely with CO –15 vol % CO_2 mixed gases for different temperatures at various magnifications are shown in Figure 8. At 916 K, the gross particle size and micrograph of the as-prepared MoO_2 keep the same as the MoO_3 raw material, compared Figure 8A1–A3 with Figure 19. Also, several small particles or nuclei are formed on the smooth platelet-shaped surface. From the blue sections shown on the top left corner in Figure 8A3, some water-waves streaks could be easily seen. As the temperature increases, the gross characteristic of the as-prepared MoO_2 is typically maintained and the smooth surface is still embedded with many small nuclei, as shown in Figure 8B1–B3. The images obtained at higher temperatures (932 and 948 K) are almost the same as those obtained at lower temperatures (901 and 916 K), all of which included both smooth surface and small nuclei as well as the water-waves streaks. To identify the possible phase compositions for the small nuclei, the back-scattering technology is adopted and the experimental results are shown in Figure 9. It can be seen that the colors for the smooth surface and small nuclei have some differences, suggesting that the main element distributions are different, which can be further verified by the energy dispersive X-ray spectroscopy (EDS) results shown in Table 2 (illustrated in Figure 9). The smooth surface and small nuclei can be identified to be MoO_2 and MoO_xC_y , respectively. All in all, the morphologies obtained in the current work have no obvious relationship with the reaction temperature in the temperature range of 901–948 K.

Figure 10 shows the FE-SEM images of reaction products obtained by reducing high-purity MoO_3 with CO –15 vol % CO_2 mixed gases at 932 K for different reaction extents (defined as the ratio of mass loss ratio of sample at time t to the theoretical maximum mass loss ratio from MoO_3 to MoO_2). When the reaction extent is $\alpha_1 = 0.0286$, the products almost kept the same smooth surface as the MoO_3 raw material (as seen in Figure 19) and no obvious nuclei is found (as seen in Figure 10A). When the reaction extent arrives at $\alpha_2 = 0.0895$ (the products are almost Mo_9O_{26} as shown in Figures 6 and 7), many big pores are formed on the smooth surface, which may result from the tensile stress generated due to the volume decreased during the oxygen removal. As the reaction proceeds forward ($\alpha_3 = 0.2492$, products included Mo_4O_{11} with few MoO_2 , as shown in Figures 6 and 7), small nuclei begin to form; in the meantime, liquid drops between two platelet-shaped particles can also be observed, as shown in Figure 10C. When the reaction extent reaches $\alpha_4 = 0.4965$, the amount of small nuclei and liquid drops increased even if most of the products still have a smooth surface, as shown in Figure 10D. The tendency for the increase of small nuclei is maintained when the reaction continues, as shown in Figure 10E. After the reaction completes, a larger number of small nuclei can be obviously seen on the smooth platelet-shaped surface, as displayed in Figure 10F. Furthermore, cracks or pores formed in Figure 10B nearly disappeared, which may be filled with the newly as-formed liquid drops.



2: MoO_2 (PDF card No. 32-671); 3: MoO_3 (PDF card No. 5-508); 4: Mo_4O_{11} (PDF card No. 5-337); 5: Mo_9O_{26} (PDF card No. 12-753)

Figure 6. XRD patterns of reaction products obtained by reducing high-purity MoO_3 with CO–15 vol % CO_2 mixed gases at 932 K for different reaction extents (defined as the ratio of mass loss ratio of sample at time t to the theoretical maximum mass loss ratio from MoO_3 to MoO_2). (a) $\alpha_1 = 0.0286$; (b) $\alpha_2 = 0.0895$; (c) $\alpha_3 = 0.2492$; (d) $\alpha_4 = 0.4965$; (e) $\alpha_5 = 0.8473$; (f) $\alpha_6 = 1$. (α represents the reaction extent, $\alpha = 1$ means reacting completely).

3. DISCUSSION

3.1. Reduction Mechanism. As can be known from Figures 1 and 2, reduction of MoO_3 with CO–15 vol % CO_2 mixed gases in the range of room temperature to 1550 K can be mainly

divided into three stages: the first is reducing MoO_3 into MoO_2 ($\text{MoO}_3 \rightarrow \text{MoO}_2$, $T_1 < T < T_2$), followed by carburizing MoO_2 into Mo_2C ($\text{MoO}_2 \rightarrow \text{Mo}_2\text{C}$, $T_2 < T < T_3$), and the last stage is to generate metallic Mo ($\text{Mo}_2\text{C} \rightarrow \text{Mo}$, $T_4 < T < T_5$). Herein, T_1 ,

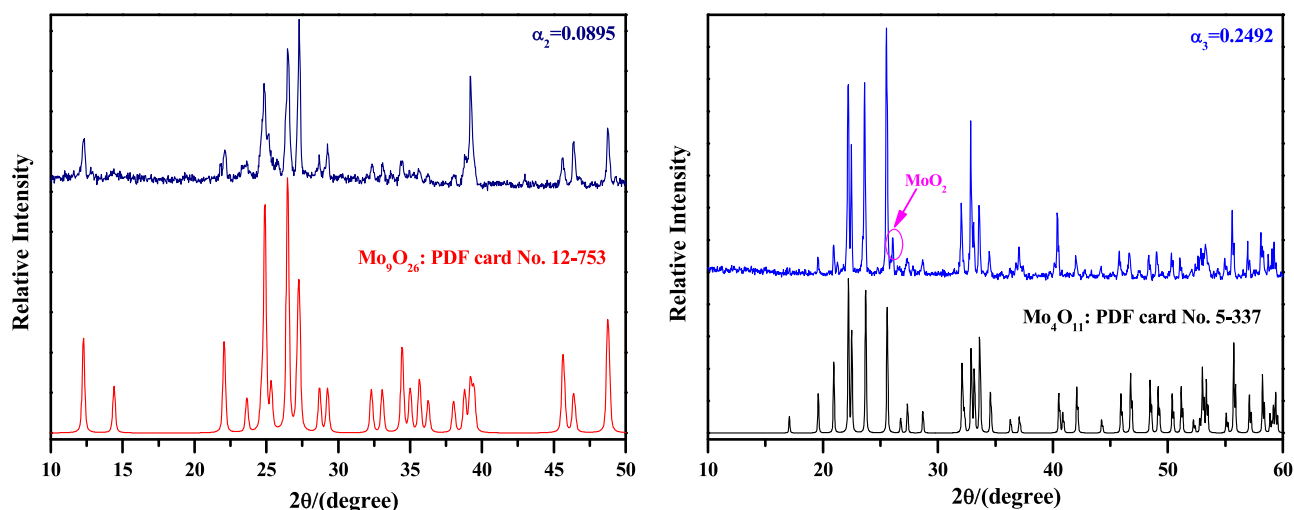
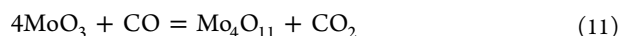
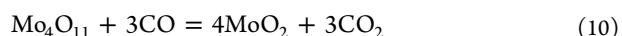
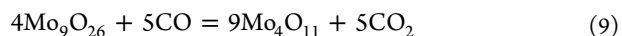


Figure 7. XRD patterns of reaction products obtained by reducing high-purity MoO_3 with CO–15 vol % CO_2 mixed gases at 932 K at the reaction extents of 0.0895 and 0.2492. Standard PDF card Nos 12-753 and 5-337 were also given as the references.

T_2 , T_3 , T_4 , and T_5 are the experimental values which vary with heating rates, as shown in Table 1. That is to say, lower temperature is beneficial for the formation of MoO_2 , higher temperature for Mo, and temperatures between them contribute to the formation of Mo–C compounds. The current results can be further proved by the phase diagram of CO– MoO_3 at 1 atm total pressure, as shown in Figure 11, which is calculated by the thermodynamic software FactSage 7.0 (ThermFact Ltd., Montreal, Canada).²³ One of the difference is that the critical transformation temperatures from MoO_2 to Mo_2C and Mo_2C to Mo of the experimental data shown in Table 1 are larger than those of the theoretical values shown in Figure 11 (1019 vs 907 K, and 1443 vs 1343 K, respectively). Those deviations resulted from the dynamic condition and the nonequilibrium behavior of the present experimental procedures.

As to the first stage ($\text{MoO}_3 \rightarrow \text{MoO}_2$) mentioned above, some new and interesting phenomena are found by deeper investigation. From the XRD analyses (Figures 6 and 7), it is found that this stage can be further divided into three minor steps, i.e., MoO_3 is first reduced to Mo_9O_{26} ($\text{MoO}_3 \rightarrow \text{Mo}_9\text{O}_{26}$, as shown in eq 8), then to Mo_4O_{11} ($\text{Mo}_9\text{O}_{26} \rightarrow \text{Mo}_4\text{O}_{11}$, as shown in eq 9), and finally to MoO_2 ($\text{Mo}_4\text{O}_{11} \rightarrow \text{MoO}_2$, as shown in eq 10). For expression convenience, those three minor steps are defined as one-step, two-step, and three-step reactions, respectively. The formations of Mo_9O_{26} and Mo_4O_{11} can also be supported by Figure 11, from which it can be known that Mo_9O_{26} and Mo_4O_{11} as the intermediate products are indeed formed during the reduction process. However, other suboxide, such as Mo_8O_{23} , is not detected in Figures 6 and 7, which may be due to its small amount. Herein, according to our previous work,^{12,18} Mo_4O_{11} is the only intermediate product produced in the reduction process of MoO_3 with pure CO gas. However, both Mo_9O_{26} and Mo_4O_{11} are detected in this work, even nearly pure Mo_9O_{26} and Mo_4O_{11} are obtained when the reaction extents are 0.0895 and 0.2492, respectively. The possible reasons may be explained as follows: when pure CO is used, reaction ratios for eqs 8–10 are all very fast but differ from each other; the newly as-formed Mo_9O_{26} could rapidly be reduced to Mo_4O_{11} ; in other words, the reaction ratios for eq 9 are much faster than those for eq 8, which would make Mo_9O_{26} exhausted and hardly accumulated, and then Mo_9O_{26} could not be detected in the XRD patterns, showing that MoO_3 was reduced to

Mo_4O_{11} directly, as shown in eq 11. However, when CO–15 vol % CO_2 mixed gases (low CO partial pressure) is used, the reaction ratios for eqs 8–10 are all decreased. The lower the CO partial pressure is, the lower the reaction ratio will be. Also, it may be deduced that, in this case, the reaction ratio for eq 8 is much faster than that for eq 9, instead. And then, eq 9 can be even ignored at this initial period (α in the range of 0–0.1111). After MoO_3 is reduced to Mo_9O_{26} completely, eq 9 begins. Thereafter, the reaction ratio for eq 9 is also very faster than that for eq 10; at this moment, eq 10 can also be ignored. Similarly, after Mo_9O_{26} is reduced to Mo_4O_{11} completely, eq 10 begins. According to the analysis, it can be concluded that eqs 8–10 are independent of each other. Only when the last reaction finishes, the next starts. Combining the current experimental results and refs 12, 18, it can also be deduced that low CO partial pressure is beneficial for the formation of Mo_9O_{26} , while high CO partial pressure, for Mo_4O_{11} and MoO_2 . Therefore, the current paper would also provide an important guide role for the preparation of pure Mo_9O_{26} and Mo_4O_{11} . The corresponding reaction sequences are summarized in Figure 12.



On the other hand, it can be found that particles size of the as-prepared MoO_2 are much larger than that of used MoO_3 raw materials, as comparing Figures 8 and 10 with Figure 19. Also, numerous small nuclei are generated on the surface. These phenomena can be explained as follows: when CO–15 vol % CO_2 mixed gases are used, the reduction of MoO_3 to Mo_9O_{26} begins first, and the diffusion of reducing gas CO and release of product gas CO_2 will lead to the formation of pores or cracks on the surface, as shown in Figure 10B. After MoO_3 is reduced to Mo_9O_{26} completely, the reduction of Mo_9O_{26} to Mo_4O_{11} starts. At this time, CO_2 is still produced and released, and pores still existed. Besides, several small nuclei will be generated due to the formation of eutectic between Mo_4O_{11} and other Mo–C compounds (see Table 2 and illustrated in Figure 9), which has a much lower melting point (about 683 K), as can be supported by Figure 11. The formation of MoO_xC_y is also reported in other refs 24–26, in which hydrocarbon compounds were used as the

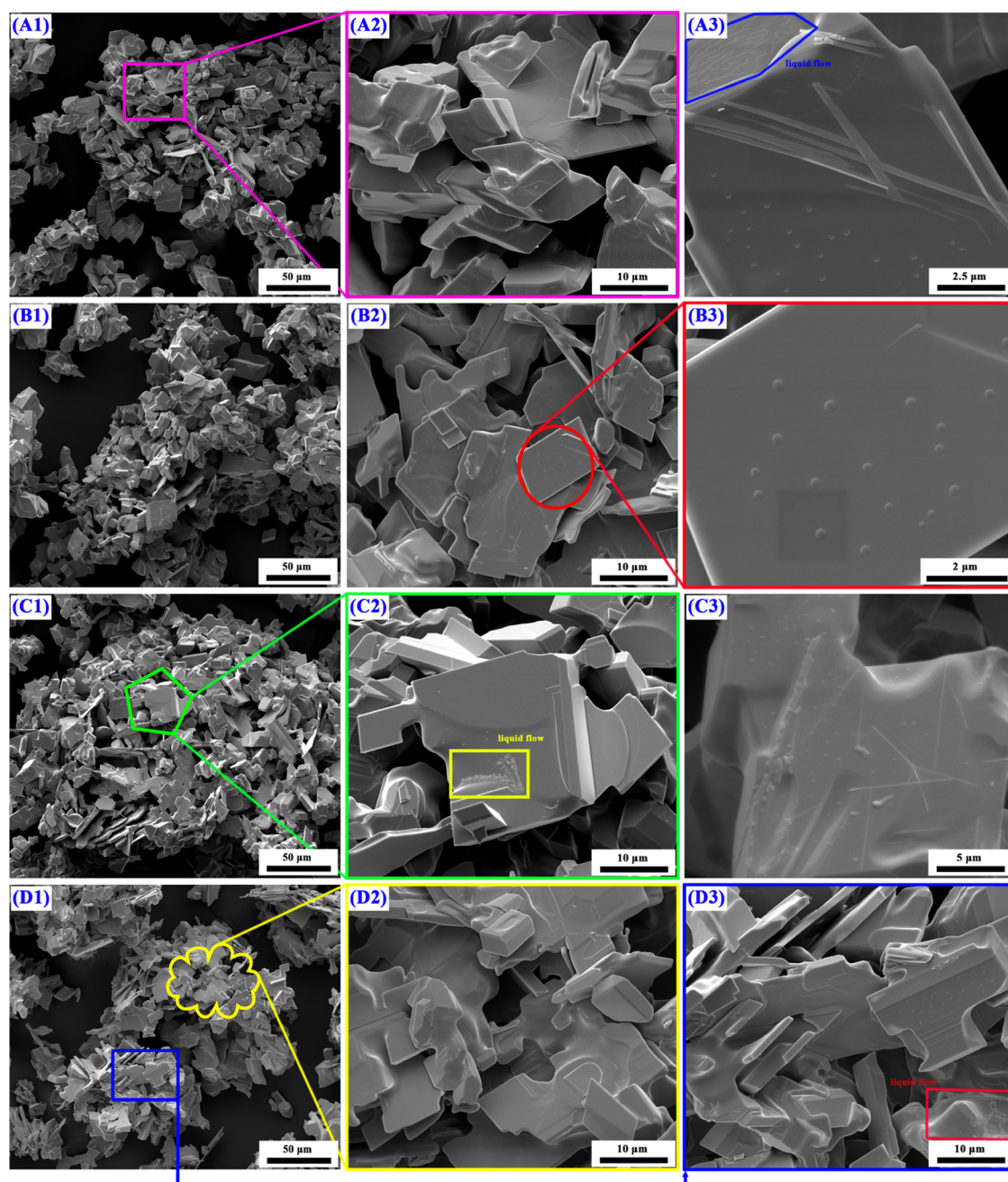


Figure 8. FE-SEM images of reaction products obtained by reducing high-purity MoO_3 completely with CO –15 vol % CO_2 mixed gases at different reaction temperatures: (A1), (A2), and (A3) 901 K; (B1), (B2), and (B3) 916 K; (C1), (C2), and (C3) 932 K; and (D1), (D2), and (D3) 948 K. (1, 2, and 3 represent different magnification times).

reducing gases. Recently, the generation of MoO_xN_y during the NH_3 reduction of the Mo – O compound has also been reported,²⁷ and the nuclei of MoO_xN_y was also very small and the morphology resembled liquid flow, which is very similar to the current experimental results. Thus, the hypothesis for the formation of the MoO_xC_y compound is reasonable in the present paper. As the reaction proceeds forward, the amount of eutectic will also be increased. Meantime, the reduction of MoO_3 to MoO_2 by CO –15 vol % CO_2 mixed gases is an exothermic reaction (see Figure 2), which will release amounts of heat and increase the local temperature, further contributing to the melting of the lower-melting-point eutectic and resulting in the sticking of different particles. The small liquid drops, in most of the time, will flow into the pores formed in the earlier

stage. Therefore, nonporous and much larger MoO_2 powder will be formed finally. The corresponding reaction mechanism can be briefly described in Figure 13.

3.2. Kinetic Analyses. From the results of Figure 3, it is found that the total reduction of MoO_3 to MoO_2 by the CO –15 vol % CO_2 mixed gases can be roughly divided into two obvious parts according to the reaction extent, i.e., from 0 to 0.1111 and 0.1111 to 1. According to the XRD results shown in Figures 6 and 7, however, it can be divided into three minor steps: (1) from MoO_3 to Mo_9O_{26} , (2) from Mo_9O_{26} to Mo_4O_{11} , and (3) from Mo_4O_{11} to MoO_2 . From the kinetic curve results, it can be known that the last two stages (2 and 3) have no obvious demarcation point, so the kinetic analyses are conducted based on the reaction extent. Herein, the model fitting method is used,

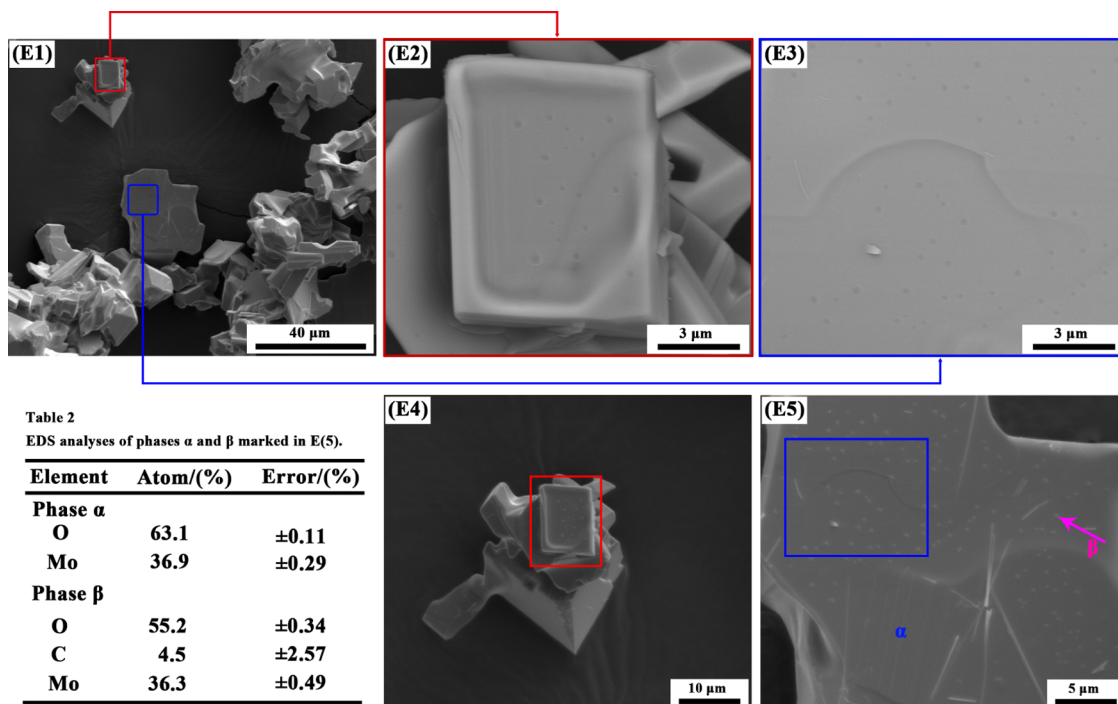


Figure 9. Images and EDS results of reaction products obtained by reducing high-purity MoO_3 completely with CO –15 vol % CO_2 mixed gases at 932 K. (E1), (E4), and (E5) SEM images; (E2) and (E3) backscattering micrographs.

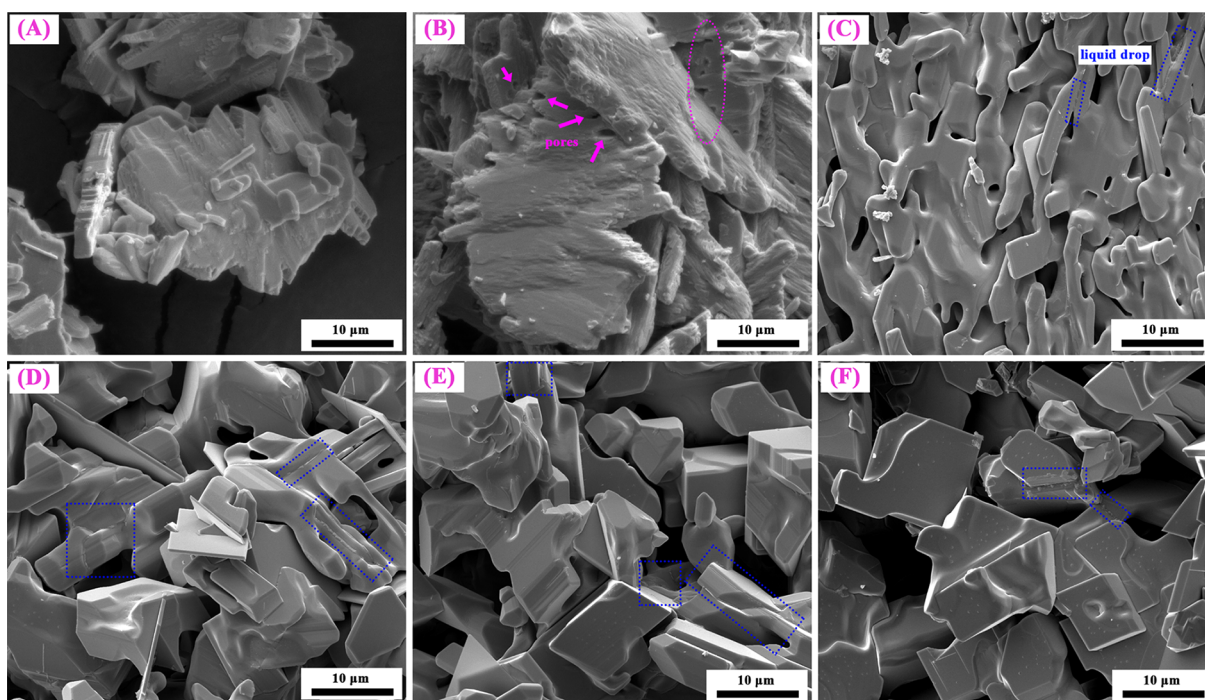


Figure 10. FE-SEM images of reaction products obtained by reducing high-purity MoO_3 with CO –15 vol % CO_2 mixed gases at 932 K for different reaction extents (defined as the ratio of mass loss ratio of sample at time t to the theoretical maximum mass loss ratio from MoO_3 to MoO_2). (A) $\alpha_1 = 0.0286$; (B) $\alpha_2 = 0.0895$; (C) $\alpha_3 = 0.2492$; (D) $\alpha_4 = 0.4965$; (E) $\alpha_5 = 0.8473$; (F) $\alpha_6 = 1$. (α represents the reaction extent, $\alpha = 1$ means reacting completely).

and the rate expressions of different gas–solid reaction models are listed in refs 28–30.

3.2.1. From 0 to 0.1111. As can be seen from Figure 10B, numerous pores and cracks are generated on the surface of products, which are beneficial for the diffusion of gases, so diffusion of gases could not be the rate-controlling step. In

addition, the nucleation and growth process may also not be the rate-controlling step because of the nearly linear kinetics curves. Therefore, the chemical reaction between the interfaces of MoO_3 and Mo_9O_{26} should be considered. By attempting different models, it is found that the chemical reaction model, as described by eq 12, can best fit the experimental data, and the

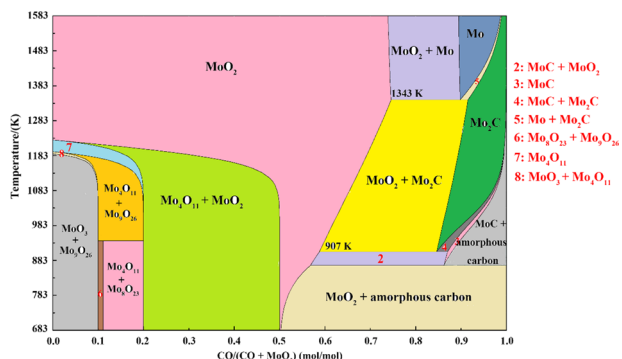


Figure 11. Stable gaseous and solid reaction products after equilibration of different molar ratios of CO and (CO + MoO₃) at 1 atm total pressure.

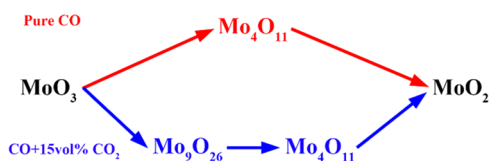


Figure 12. Schematic illustrating the reaction pathways of MoO₃ with pure CO and CO–15 vol % CO₂ mixed gases.

corresponding calculated results are shown in Figure 14. The slope of each straight line determined the reaction rate constant, k (a function of temperature, as described by the Arrhenius equation (see eq 13), where A is the preexponential factor (min^{-1}), ΔE is the activation energy (J/mol), R is the gas constant (8.314 J/(mol K)), and T is the absolute temperature (K), which increased with the increase of reaction temperature

$$\alpha = kt \quad (12)$$

$$k = A \exp\left(-\frac{\Delta E}{RT}\right) \quad (13)$$

According to eq 13, one can easily obtain

$$\ln k = -\frac{\Delta E}{R} \times \frac{1}{T} + \ln A \quad (14)$$

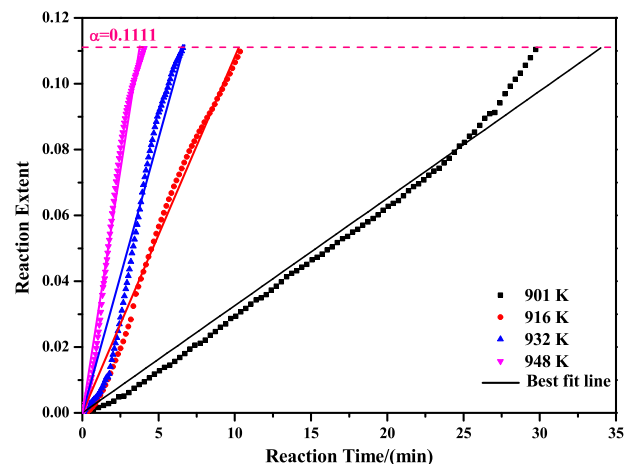


Figure 14. Plot of reaction extent α vs reaction time t (α in the range of 0–0.1111).

Substituting different rate constants k obtained from Figure 14 into eq 14, the corresponding results can be obtained, as shown in Figure 15. From Figure 5 it can be observed that the

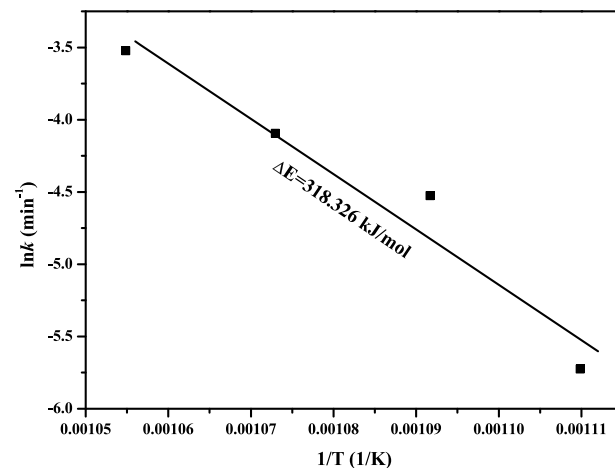


Figure 15. Arrhenius plot for the reduction of MoO₃ to Mo₉O₂₆.

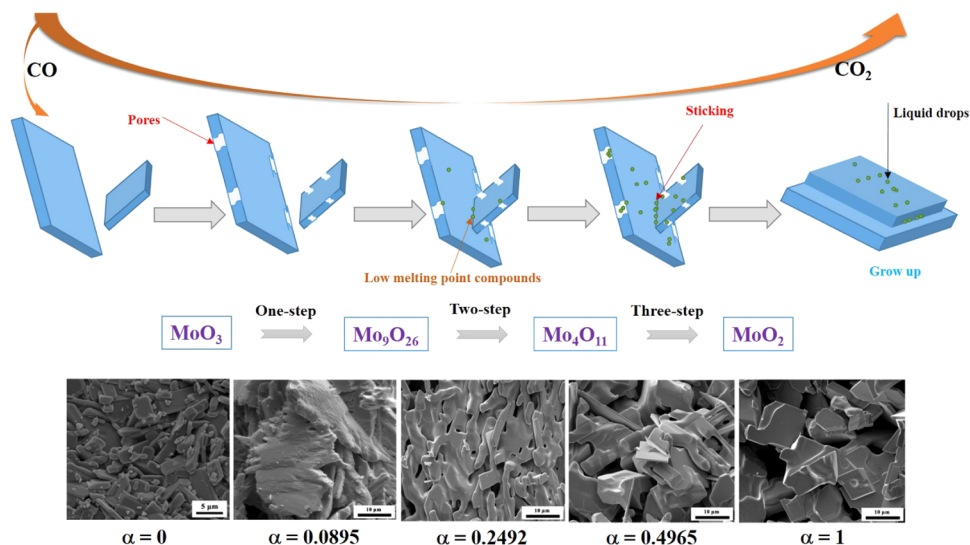


Figure 13. Proposed possible reaction mechanism diagram for the reduction process of MoO₃ to MoO₂ by the CO–15 vol % CO₂ mixed gases.

experimental data agree well with the Arrhenius equation, which further suggests that reduction from MoO_3 to Mo_9O_{26} obeys the chemical reaction model in the temperature range of 901–948 K. Moreover, an activation energy of 318.326 kJ/mol is extracted, and then the reaction extent α can be expressed by eq 15

$$\alpha = 0.1111 \times 1.14 \times 10^{16} \exp\left(-\frac{318326}{RT}\right)t \quad (15)$$

3.2.2. From 0.1111 to 1. From Figure 10C, it can be found that pores still existed in this period of time. As reaction proceeds, pores gradually disappeared. Thereafter, many small liquid drops are formed on the surface, which will hinder the diffusion of gases seriously. However, according to the linear kinetics curves shown in Figure 3, it may be deduced that chemical reaction is still the dominating rate-controlling step (diffusion may also work in the very latter period). Similarly, it is found that eq 12 can also best fit the experimental data at the reaction extent between 0.1111 and 1 (from Mo_9O_{26} to MoO_2 ; herein, the last two steps are analyzed together due to the well linear kinetic curves and no obvious demarcation point appears), as shown in Figure 16. In the meantime, substituting different

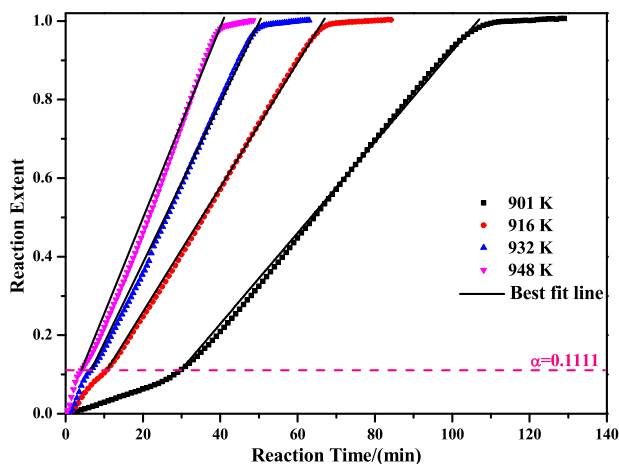


Figure 16. Plot of reaction extent α vs reaction time t (α in the range of 0.1111–1).

slopes obtained from Figure 16 into eq 14, the corresponding Arrhenius plot can also be calculated, as displayed in Figure 17, from which activation energy of 112.047 kJ/mol is easily extracted. Therefore, the algebraic expression of the reaction extent α in the range of 0.1111–1 can be obtained as shown in eq 16

$$\alpha = 0.1111 + 0.8889 \times 3.75 \times 10^4 \exp\left(-\frac{112047}{RT}\right) (t - t_0) \quad (16)$$

where t_0 is the time related to the reaction extent of 0.1111 at a desired temperature.

The activation energies extracted for the reduction reaction from MoO_3 to Mo_9O_{26} is much larger than that from Mo_9O_{26} to MoO_2 (318.326 vs 112.047 kJ/mol), from which it may be mistaken for a lower reaction rate in the former. However, from the kinetics curve (see Figure 3), it can be found that the reaction rate in the range of 0–0.1111 is also very fast, especially at higher temperatures. In this case, it can also be observed that the preexponential factors obtained in the range of 0–0.1111 is

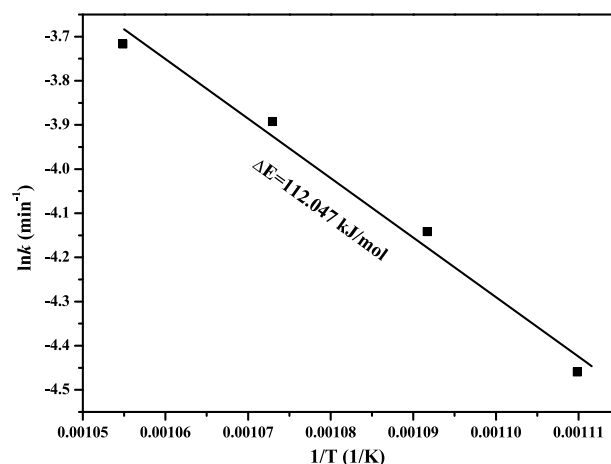


Figure 17. Arrhenius plot for the reduction of Mo_9O_{26} to MoO_2 .

much larger than that obtained in the range of 0.1111–1 (1.14×10^{16} vs 3.75×10^4), which indicates that the collision frequency in the primary period is more intense and then improves the reaction rate in turn, which is in good agreement with the kinetic compensation effect.³¹

4. CONCLUSIONS

In this work, reduction of high-purity MoO_3 with CO–15 vol % CO_2 mixed gases is investigated by the nonisothermal and isothermal thermogravimetric experiments. The following conclusions can be drawn:

1. Temperature has a significant influence on the product composition: when the temperature is low, the main product is MoO_2 ; on increasing the reaction temperature, the main product will turn to be Mo_2C ; on further increasing the temperature ($T > T_4 = 1443$ K), metallic Mo will be generated.
2. Reduction of MoO_3 to MoO_2 by the CO–15 vol % CO_2 mixed gases is proceeded following a three-step reaction processes with the formation of intermediate products of Mo_9O_{26} and Mo_4O_{11} . The reaction sequences of $\text{MoO}_3 \rightarrow \text{Mo}_9\text{O}_{26} \rightarrow \text{Mo}_4\text{O}_{11} \rightarrow \text{MoO}_2$ are proposed.
3. The final products always keep the same platelet shape and smooth morphology as the MoO_3 raw material. However, the particle size of products will be increased due to the formation of lower-melting-point eutectic and the sticking of particles.
4. The rate-controlling step for the reduction of MoO_3 to Mo_9O_{26} and Mo_9O_{26} to MoO_2 (mainly from Mo_4O_{11} to MoO_2) is both interfacial chemical reactions. The extracted activation energies are 318.326 and 112.047 kJ/mol, respectively.

5. MATERIALS AND EXPERIMENTAL PROCEDURES

5.1. Materials. High-purity MoO_3 purchased from Jindui-cheng Molybdenum Co., Ltd., Xi'an, China, was used for the experiments. Figure 18 shows the X-ray diffraction patterns of the studied raw material. As can be easily seen, the material has a very high purity without any impurities. The studied MoO_3 powder belongs to the thermodynamically stable orthorhombic phase, α - MoO_3 , which can also be deduced according to the information of PDF card No. 5-508. The images of the raw materials are presented in Figure 19, from which it can be known that the powders are composed of many platelet-shaped particles

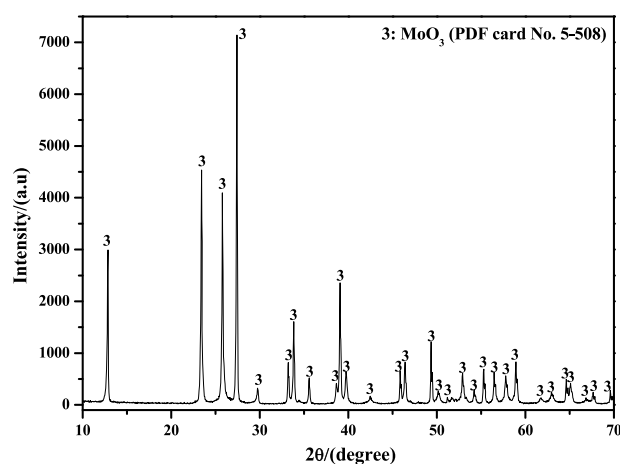


Figure 18. XRD pattern of studied MoO₃ powder.

with some small ones attached on the smooth surface. In addition, most of the small particles are agglomerated together with each other to form a big block.

5.2. Experimental Procedures. To monitor the weight loss continuously during the reduction process, a thermal analysis system (HTC-3, Beijing Hengjiu Instrument Ltd., Beijing), which includes a thermogravimetry (TG) microbalance with a precision of $\pm 0.1 \mu\text{g}$, was used. The corresponding schematic diagram of the experimental apparatus is shown in the literature.¹⁸ To establish the potential isothermal experimental temperatures, a series of nonisothermal thermogravimetry differential thermal analysis (TG-DTA) experiments were carried out first. During the nonisothermal experimental processes, about 40 mg of MoO₃ powder was loaded into an alumina crucible ($\phi 7 \text{ mm} \times 2 \text{ mm}$) and placed into a furnace. The CO–15 vol % CO₂ mixed gases were then introduced into the reaction tube to drive the air out before the furnace was heated from ambient temperature (about 298 K) to 1550 K at different heating rates (5, 10, 15, and 20 K/min). When the temperature reached 1550 K, the furnace was cooled down to room temperature again in the same gas atmosphere (CO–15 vol % CO₂ mixed gases).

After establishing the potential isothermal experimental temperatures according to the nonisothermal TG-DTA curves, the isothermal experiments were conducted subsequently. In each experimental run, about 40 mg of MoO₃ powder was filled into the alumina crucible and then placed in a flat temperature

zone of the furnace. Due to the stability of high-purity α -MoO₃ at low temperature (α -MoO₃ will not evaporate or sublimate when the temperature is below 973 K),^{32,33} air gas was selected to be introduced into the system first. When the furnace was heated from room temperature to the desired temperatures (901, 916, 932, and 948 K) at a heating rate of 10 K/min, air gas switched to the reducing gases (CO–15 vol % CO₂ mixed gases) to start the reduction reaction. After reacting for a suitable period of time or completely, the furnace was cooled down to room temperature again under the same gas atmosphere. The samples were then collected for further characterization.

In all of the experimental runs, a constant gas flow rate of 100 mL/min was maintained during the reaction process. CO–15 vol % CO₂ mixed gases were synthesized by Wuhan Minghui Gas Technology Co., Ltd., Wuhan, China. X-ray powder diffraction (XRD; D8 Advance, AXS Corporation, Bruker, Germany, Cu K α filtered radiation, and operated at 30 kV and 20 mA at a scanning speed of 10°/min) was used to identify the phase compositions. Field emission scanning electron microscopy (FE-SEM; Nova 400 NanoSEM, FEI Corporation, and with an acceleration voltage of 15 kV) was used to observe the evolution laws of product morphologies during the reduction processes.

AUTHOR INFORMATION

Corresponding Authors

*E-mail: wanglu@wust.edu.cn (L.W.).

*E-mail: xuezhengliang@wust.edu.cn (Z.-L.X.).

ORCID

Lu Wang: 0000-0002-0317-2225

Notes

The authors declare no competing financial interest.

ACKNOWLEDGMENTS

The authors gratefully acknowledge the financial support for this work from the National Natural Science Foundation of China (51874214), the Special Project of Central Government for Local Science and Technology Development of Hubei Province (2019ZYYD076), National Postdoctoral Program for Innovative Talents-funded project (BX20180023), and China Postdoctoral Science Foundation-funded project (2019M650424).

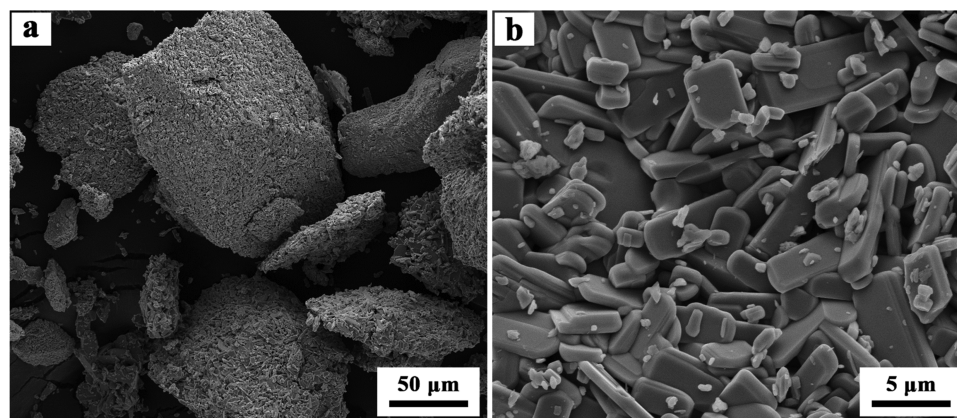


Figure 19. Images of the studied MoO₃ powder amplified (a) 1000 times and (b) 10 000 times.

REFERENCES

- (1) Kahruman, C.; Yusufoglu, I.; Oktay, E. Kinetics of oxidation of MoO₂ to MoO₃ by oxygen at elevated temperatures. *Trans. Inst. Min. Metall., Sect. C* **1999**, *108*, C8–C14.
- (2) Utigard, T. Oxidation mechanism of molybdenite concentrate. *Metall. Mater. Trans. B* **2009**, *40*, 490–496.
- (3) Lessard, J. D.; Shekhter, L. N.; Gribbin, D. G.; McHugh, L. F. Thermodynamic Analysis of Looping Sulfide Oxidation Production of MoO₂ from Molybdenite for Energy Capture and Generation. *JOM* **2013**, *65*, 1566–1572.
- (4) Chychko, A.; Teng, L.; Seetharaman, S. MoO₃ evaporation studies from binary systems towards choice of Mo precursors in EAF. *Steel Res. Int.* **2010**, *81*, 784–791.
- (5) Wang, L.; Zhang, G. H.; Xue, Z. L.; Song, C. M. Shape-controlled Preparation of Mo Powder by Temperature-programmed Reduction of MoO₃ by NH₃. *Chem. Lett.* **2019**, *48*, 475–478.
- (6) Dang, J.; Zhang, G. H.; Chou, K. C.; Reddy, R. G.; He, Y.; Sun, Y. Kinetics and mechanism of hydrogen reduction of MoO₃ to MoO₂. *Int. J. Refract. Met. Hard Mater.* **2013**, *41*, 216–223.
- (7) Wang, L.; Zhang, G. H.; Chou, K. C. Mechanism and kinetic study of hydrogen reduction of ultra-fine spherical MoO₃ to MoO₂. *Int. J. Refract. Met. Hard Mater.* **2016**, *54*, 342–350.
- (8) Blanco, E.; Sohn, H. Y.; Han, G.; Hakobyan, K. Y. The kinetics of oxidation of molybdenite concentrate by water vapor. *Metall. Mater. Trans. B* **2007**, *38*, 689–693.
- (9) Hakobyan, K.; Sohn, H.; Hakobyan, A.; Bryukvin, V.; Leontiev, V.; Tsibin, O. The oxidation of molybdenum sulphide concentrate with water vapour Part 2—Macrokinetics and mechanism. *Miner. Process. Extr. Metall.* **2007**, *116*, 155–158.
- (10) Wang, L.; Bu, C. Y.; Zhang, G. H.; Jiang, T.; Chou, K. C. Preparation of MoO₂ by the Solid State Reaction Between MoS₂ and MoO₃. *JOM* **2016**, *68*, 1031–1036.
- (11) Wilkomirsky, I.; Sáez, E. Kinetics and mechanism of formation of MoO₂ by solid state reaction between MoS₂ and MoO₃. *Can. Metall. Q* **2019**, *1*–10.
- (12) Wang, L.; Bu, C. Y.; Zhang, G. H.; Wang, J. S.; Chou, K. C. Study of the Reduction of Industrial Grade MoO₃ Powders with CO or CO-CO₂ Gases to Prepare MoO₂. *Metall. Mater. Trans. B* **2017**, *48*, 2047–2056.
- (13) Lemaitre, J.; Vidick, B.; Delmon, B. Control of the catalytic activity of tungsten carbides: I. Preparation of highly dispersed tungsten carbides. *J. Catal.* **1986**, *99*, 415–427.
- (14) Valendar, H. M.; Rezaie, H.; Samim, H.; Barati, M.; Razavizadeh, H. Reduction and carburization behavior of NiO–WO₃ mixtures by carbon monoxide. *Thermochim. Acta* **2014**, *590*, 210–218.
- (15) Alonso, F. N.; Morales, M. Z.; Salas, A. U.; Becerril, J. B. Tungsten trioxide reduction-carburization with carbon monoxide-carbon dioxide mixtures: kinetics and thermodynamics. *Int. J. Miner. Process.* **1987**, *20*, 137–151.
- (16) Wu, Y.; Dang, J.; Lv, Z.; Zhang, R. The preparation of tungsten carbides and tungsten powders by reaction of tungsten trioxide with methanol. *Int. J. Refract. Met. Hard Mater.* **2018**, *76*, 99–107.
- (17) Dang, J.; Zhang, G. H.; Wang, L.; Chou, K. C.; Pistorius, P. C. Study on reduction of MoO₂ powders with CO to produce Mo₂C. *J. Am. Ceram. Soc.* **2016**, *99*, 819–824.
- (18) Wang, L.; Zhang, G. H.; Chou, K. C. Preparation of Mo₂C by reducing ultrafine spherical β-MoO₃ powders with CO or CO-CO₂ gases. *J. Aust. Ceram. Soc.* **2018**, *54*, 97–107.
- (19) Schulmeyer, W. V.; Ortner, H. M. Mechanisms of the hydrogen reduction of molybdenum oxides. *Int. J. Refract. Met. Hard Mater.* **2002**, *20*, 261–269.
- (20) Ressler, T.; Jentoft, R. E.; Wienold, J.; Günter, M. M.; Timpe, O. In situ XAS and XRD studies on the formation of Mo suboxides during reduction of MoO₃. *J. Phys. Chem. B* **2000**, *104*, 6360–6370.
- (21) Majumdar, S.; Sharma, I.; Samajdar, I.; Bhargava, P. Kinetic studies on hydrogen reduction of MoO₃ and morphological analysis of reduced Mo powder. *Metall. Mater. Trans. B* **2008**, *39*, 431–438.
- (22) Lalik, E. Kinetic analysis of reduction of MoO₃ to MoO₂. *Catal. Today.* **2011**, *169*, 85–92.
- (23) Bale, C.; Bélisle, E.; Chartrand, P.; Decterov, S.; Eriksson, G.; Hack, K.; Jung, I. H.; Kang, Y. B.; Melançon, J.; Pelton, A. FactSage thermochemical software and databases—recent developments. *Calphad* **2009**, *33*, 295–311.
- (24) Hanif, A.; Xiao, T.; York, A. P.; Sloan, J.; Green, M. L. Study on the structure and formation mechanism of molybdenum carbides. *Chem. Mater.* **2002**, *14*, 1009–1015.
- (25) Xiao, T. C.; York, A. P.; Williams, V. C.; Al-Megren, H.; Hanif, A.; Zhou, X. Y.; Green, M. L. Preparation of molybdenum carbides using butane and their catalytic performance. *Chem. Mater.* **2000**, *12*, 3896–3905.
- (26) Wang, X. H.; Hao, H. L.; Zhang, M. H.; Li, W.; Tao, K. Y. Synthesis and characterization of molybdenum carbides using propane as carbon source. *J. Solid State Chem.* **2006**, *179*, 538–543.
- (27) Wang, L.; Zhang, G. H.; Chou, K. C. Study on reduction reaction of MoO₂ powder with NH₃. *J. Am. Ceram. Soc.* **2017**, *100*, 1368–1376.
- (28) Ebrahimi-Kahrizangi, R.; Abbasi, M. H.; Saidi, A. Mechanochemical effects on the molybdenite roasting kinetics. *Chem. Eng. J.* **2006**, *121*, 65–71.
- (29) Vyazovkin, S.; Wight, C. A. Model-free and model-fitting approaches to kinetic analysis of isothermal and nonisothermal data. *Thermochim. Acta.* **1999**, *340*, 53–68.
- (30) Kim, B. S.; Kim, E. Y.; Jeon, H. S.; Lee, H. I.; Lee, J. C. Study on the reduction of molybdenum dioxide by hydrogen. *Mater. Trans.* **2008**, *49*, 2147–2152.
- (31) Zsakó, J. The kinetic compensation effect. *J. Therm. Anal. Calorim.* **1976**, *9*, 101–108.
- (32) Norman, J.; Staley, H. G. Thermodynamics of the dimerization and trimerization of gaseous tungsten trioxide and molybdenum trioxide. *J. Chem. Phys.* **1965**, *43*, 3804–3806.
- (33) Wang, L.; Zhang, G. H.; Dang, J.; Chou, K. C. Oxidation roasting of molybdenite concentrate. *Trans. Nonferrous Met. Soc. China* **2015**, *25*, 4167–4174.